

Deep *Chandra* survey of the Small Magellanic Cloud. III. Formation efficiency of high-mass X-ray binaries

VALLIA ANTONIOU,^{1,2} ANDREAS ZEAS,^{3,1} JEREMY J. DRAKE,¹ CARLES BADENES,⁴ FRANK HABERL,⁵
NICHOLAS J. WRIGHT,⁶ JAESUB HONG,¹ ROSANNE DI STEFANO,¹ TERRANCE J. GAETZ,¹ KNOX S. LONG,⁷
PAUL P. PLUCINSKY,¹ MANAMI SASAKI,⁸ BENJAMIN F. WILLIAMS,⁹ AND P. FRANK WINKLER¹⁰
(SMC XVP COLLABORATION)

¹*Harvard-Smithsonian Center for Astrophysics 60 Garden Street, Cambridge, MA 02138, USA*

²*Department of Physics and Astronomy, Box 41051, Science Building, Texas Tech University, Lubbock, TX 79409, USA*

³*Physics Department and Institute of Theoretical and Computational Physics, University of Crete, 71003 Heraklion, Crete, Greece;
Foundation for Research and Technology-Hellas, 71110 Heraklion, Crete, Greece*

⁴*Department of Physics and Astronomy and Pittsburgh Particle Physics, Astrophysics and Cosmology Center, University of Pittsburgh,
Pittsburgh, PA 15260, USA*

⁵*Max-Planck-Institut für extraterrestrische Physik, Giessenbachstrae, D-85748 Garching, Germany*

⁶*Astrophysics Group, Keele University, Keele, ST5 5BG, UK*

⁷*Space Telescope Science Institute, 3700 San Martin Drive, Baltimore, MD 21218, USA*

⁸*Dr. Karl Remeis-Sternwarte, Erlangen Centre for Astroparticle Physics, Friedrich-Alexander-Universitt Erlangen-Nrnberg,
Sternwartstrasse 7, D-96049 Bamberg, Germany*

⁹*Astronomy Department, University of Washington, Box 351580, Seattle, WA 98195, USA*

¹⁰*Department of Physics, Middlebury College, Middlebury, VT 05753, USA*

Submitted to ApJ

ABSTRACT

We have compiled the most complete census of High-Mass X-ray Binaries (HMXBs) in the Small Magellanic Cloud with the aim to investigate the formation efficiency of young accreting binaries in its low metallicity environment. In total, we use 127 X-ray sources with detections in our *Chandra* X-ray Visionary Program (XVP), supplemented by 14 additional (likely and confirmed) HMXBs identified by Haberl & Sturm (2016) that fall within the XVP area, but are not either detected in our survey (9 sources) or matched with any XVP source that has at least one OB counterpart in the OGLE-III catalog (5 sources). Specifically, we examine the number ratio of the HMXBs $N(\text{HMXBs})$ to (a) the number of OB stars, (b) the local star-formation rate (SFR), and (c) the stellar mass produced during the specific star-formation burst, all as a function of the age of their parent stellar populations. Each of these indicators serves a different role, but in all cases we find that the HMXB formation efficiency increases as a function of time (following a burst of star formation) up to $\sim 40\text{--}60$ Myr, and then gradually decreases. The peak formation efficiency $N(\text{HMXB})/\text{SFR}$ is $(49 \pm 14) [10^{-5} \text{ M}_{\odot}/\text{yr}]^{-1}$, in good agreement with previous estimates of the average formation efficiency in the broad $\sim 20\text{--}60$ Myr age range. The frequency of HMXBs is a factor of $8\times$ higher than at ~ 10 Myr, and $4\times$ higher than at ~ 260 Myr, i.e. at earlier and later epochs, respectively.

Keywords: Magellanic Clouds — galaxies: star formation — stars: early-type — stars: emission-line, Be — X-rays: binaries — stars: neutron

1. INTRODUCTION

X-ray binaries (XRBs) are our main tool for studying the populations of compact objects in galaxies, and the

formation and evolution of intermediate and higher mass binary stellar systems. Systematic studies of nearby galaxies have provided initial estimates of the formation rate of XRBs as a function of the SFR and stellar mass (M_{\star}) of their host galaxies (Lehmer et al. 2010, Mineo et al. 2012). A strong dependence of the XRB formation rate on age and metallicity has been predicted (Dray

2006, Linden et al. 2010, Fragos et al. 2013); however, we are only now starting to probe the details of this connection (Shtykovskiy & Gilfanov 2005, Antoniou et al. 2010, Williams et al. 2013, Antoniou & Zezas 2016). The Small Magellanic Cloud (SMC) is the ideal target to study the dependence of the formation efficiency of XRBs on the age of their parent stellar population. It is our second nearest ($D=61.9\pm0.6$ kpc; de Grijs & Bono 2015) star-forming galaxy, and offers a clear picture of its spatially-resolved star-formation (SF) history (Harris & Zaritsky 2004, hereafter [HZ04]). Furthermore, it has low metallicity (Luck et al. 1998; Antoniou & Zezas 2016, and references therein), and hosts one of the largest known populations of High-Mass X-ray Binaries (HMXBs) known in a galaxy, rivaling that of the Milky Way (e.g. Coe & Kirk 2015; Haberl & Sturm 2016, hereafter [HS16]).

In order to study the HMXB populations in the SMC in detail, and in particular their connection with their parent stellar population, we performed a deep *Chandra* X-ray Visionary Project (XVP) survey of selected SMC regions chosen to sample stellar populations of different ages. The first results on the spectral and timing properties of pulsars detected in the survey fields are presented in Hong et al. (2016, 2017). In this work, we present our measurement of the formation efficiency of the SMC HMXB populations as a function of their age, the most detailed such measurement so far. In §2 we describe briefly the *Chandra* XVP SMC survey, and the source sample used, while in §3 we discuss the SF history of the regions studied, and we link the SF in each region with the XRB populations. In §4 we estimate the formation efficiency of HMXBs, and present the HMXB delay time distribution (DTD). In §5 we discuss these results and compare the different HMXB formation efficiency indicators. The most important findings are summarized in §6.

Throughout this work, we adopt a distance modulus of $(m-M)_V = 18.96\pm0.02$ mag (de Grijs & Bono 2015), $R_V = 2.74\pm0.13$ (Gordon et al. 2003), and $E(B-V)(=A_V/R_V) = 0.09\pm0.02$ mag (Udalski et al. 1999), thus the extinction A_V is estimated to be 0.25 mag, and in turn¹ $A_I = 0.12$ mag, and $E(V-I) = 0.13$ mag.

2. SURVEY DESCRIPTION AND DATA ANALYSIS

The SMC has been surveyed extensively in the X-ray band with *Einstein* (e.g. Seward & Mitchell 1981), *ROSAT* (e.g. Sasaki et al. 2000, Haberl et al. 2000), *RXTE* (e.g. Laycock et al. 2005, Corbet et al. 2009), *ASCA* (e.g. Yokogawa et al. 2003), and *XMM-*

Newton (e.g. Haberl et al. 2012, Sturm et al. 2013), with the latter yielding the most extensive survey of the galaxy down to luminosities of 5×10^{33} erg s⁻¹ (Haberl et al. 2012). In order to reach well within the regime of the X-ray emission of quiescent XRBs ($\sim 10^{32}$ erg s⁻¹) and obtain as complete a picture of its HMXB populations as possible, a *Chandra* XVP Program was awarded (PI A. Zezas) to perform a comprehensive survey, to a depth of 100 ks exposure, of 11 fields selected to represent young (< 100 Myr) stellar populations of different ages. These observations were performed from December 2012 to February 2014, utilizing the ACIS-I imaging mode.

In addition, we also analyzed 3 archival observations reaching the same 100 ks depth. Two of these fields (PI A. Zezas; observed in 2006) overlap partially with fields from the XVP survey, and the third is centered on NGC 346 (PI M. Corcoran; observed in 2001). Although analyses of these data have been presented elsewhere (Laycock et al. 2010 and Nazé et al. 2002, respectively), we opted to reanalyze all consistently using the latest calibrations. In Figure 1 we present a Magellanic Cloud Emission Line Survey (MCELS) $H\alpha$ image of the SMC overlaid with the observed fields, color-coded for the age of their stellar population derived using data from [HZ04].

Source detection employed *CIAO* WAVDETECT in 4 bands (broad 0.5–7.0 keV, soft 0.5–1.2 keV, medium 1.2–2.0 keV, and hard 2.0–7.0 keV) on all individual ObsIDs and the merged dataset for each field. All subsequent data analysis steps (source photometry, screening, spectral fitting, timing analysis) were performed with *ACIS Extract* (AE Version 2014may23; Broos et al. 2010, 2012). This yielded 2,393 sources down to a limiting flux of 2.6×10^{-16} erg cm⁻² s⁻¹ in the full (0.5–8.0 keV) band ($\sim 50\%$ complete at 7.94×10^{-16} erg cm⁻² s⁻¹). Further details on the survey, data analysis, and the complete source catalog² are presented in Antoniou et al. (2019, in prep).

In order to identify the HMXBs in the complete source catalog, we cross-correlated the locations of the X-ray sources with the OGLE-III catalog of stars in the SMC (Udalski et al. 2008). We used a cross-correlation radius based on Eq. 5 of Hong et al. (2005), limited to a minimum radius of 1'' based on the minimum combined positional uncertainty of the X-ray and optical catalogs. Following Antoniou et al. (2010) and Antoniou & Zezas (2016), we classified as HMXBs X-ray sources

² The limit we set on the probability of these sources of being just a background fluctuation – value of PROB_NO_SOURCE or P_B in *AE* – is 0.01.

¹ Assuming the extinction curve of Cardelli et al. (1989).

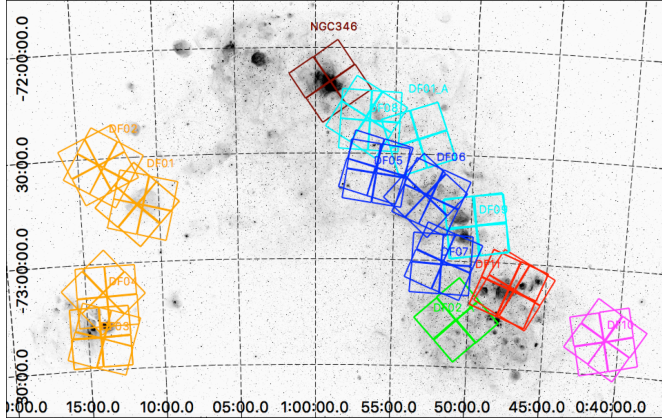


Figure 1. MCELS $H\alpha$ image (F. Winkler/Middlebury College, the MCELS Team, and NOAO/AURA/NSF) overlaid with the 14 *Chandra* fields analyzed in this work, color-coded for the ages of their parent stellar population (orange: 11 Myr, blue: 34 Myr, cyan: 42 Myr, magenta: 67 Myr). Three fields have two distinct stellar populations: DF11 (7 Myr and 42 Myr – red), DF02_A (42 Myr and 167.9 Myr – green), and NGC346 (5 Myr and 42 Myr – maroon).

with optical counterparts within the OB-star locus of the $(V, V - I)$ color-magnitude diagram (CMD). This locus is based on the location of massive stars from the spectroscopic census of the SMC (Bonanos et al. 2010). In order to account for the well-known effect that Be-XRBs (the most numerous subclass of SMC HMXBs) appear redder than OB stars due to the circumstellar disk of their Oe/Be star (e.g. Antoniou et al. 2009a, Antoniou et al. 2009b, Bonanos et al. 2010), we extended the locus to redder colors based on the locations of known HMXBs from [HS16]³ on the same CMD. We define the “extended” OB-star locus (hereafter referred simply as the OB-star locus) to lie within $V \leq 18$ mag, $I \leq 18$ mag, and $-0.4 \leq V - I \leq 0.6$ mag (Figure 2).

3. STAR-FORMATION HISTORY

A spatially-resolved SF history was derived for the SMC with a scale of $12' \times 12'$ (216.2 pc \times 216.2 pc) as part of the Magellanic Clouds Photometric Survey (MCPS [HZ04]). The SF history in each of the *Chandra* fields we adopt is the total SF history of the MCPS subregions they encompass, weighted by the fraction of the area of each MCPS subregion covered by the field.

In order to estimate the chance coincidence probability of identifying spurious matches from the OGLE-III catalog as the optical counterparts of the HMXBs, we performed extensive Monte Carlo simulations fol-

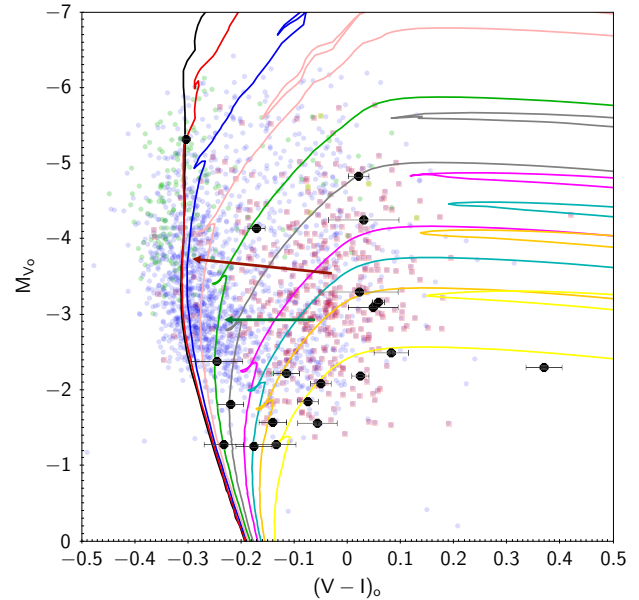


Figure 2. An example of the age determination for the HMXBs identified in field DF11 of the *Chandra* XVP survey. The extinction-corrected magnitude and color are defined as $M_{V_o} = (m - M)_V - A_V = V - 18.96 - 0.25$, and $(V - I)_o = (V - I) - E(V - I) = (V - I) - 0.13$, respectively. The underlying points are from the spectroscopic census of OB stars in the SMC (blue: B stars; green: O stars, red: Be stars, orange: Oe stars) by Bonanos et al. (2010), overlaid with the PARSEC isochrones (black: 4.5 Myr; red: 6.3 Myr; blue: 10.0 Myr; pink: 15.8 Myr; green: 25.1 Myr; grey: 39.8 Myr; magenta: 63.1 Myr; cyan: 79.4 Myr; orange: 100.0 Myr; yellow: 158.5 Myr). The two vectors, maroon and dark green, show the shift of the Be stars due to their intrinsic reddening with respect to the B stars in the [B0,B2] and [B2,B4] spectral-type bins, respectively (the start and end points of the arrows are centered at the median M_{V_o} and $(V - I)_o$ values of each population).

lowing Antoniou et al. (2009a), and Antoniou & Zezas (2016). These results indicate that for a search radius of $1''$, about 10% of the bright blue ($V \leq 16$ mag and $-0.4 \leq (V - I) \leq 0.6$ mag) matches are spurious associations, with this probability increasing to 17% and 79% for $16 < V \leq 17$ mag, and $17 < V \leq 18$ mag, respectively (Antoniou et al. 2019, in prep.). These results show that the brightest (and subsequently bluest, for objects of similar brightness) match for sources with multiple matches is the most likely optical counterpart (c.f. Antoniou et al. 2009a). Our final HMXB sample consists of candidate sources identified in this work (127 sources matched with a total of 143 early-type stars), supplemented by all additional HMXBs identified by [HS16] (likely and confirmed sources) that fall within the XVP area, but are not either detected in our survey (9 sources) or matched with any XVP source that has at least one OB counterpart in the OGLE-III cata-

³ Using the 120 high-confidence sources reported in [HS16].

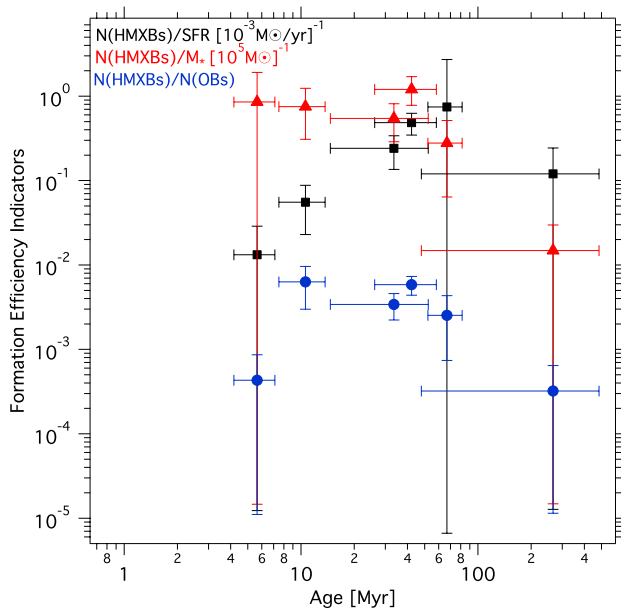


Figure 3. The following formation efficiency indicators are shown as a function of the age of their parent stellar population: $N(\text{HMXBs})$ over the SFR (black squares); $N(\text{HMXBs})$ over the stellar mass produced during the major SF burst (red triangles); $N(\text{HMXBs})/N(\text{OBs})$ in the studied fields (blue circles).

$\log(5 \text{ sources})^4$. Our final source sample comprises 141 candidate and confirmed HMXBs.

For the purpose of measuring the formation rate of HMXBs with respect to their parent stellar populations, when an HMXB falls within two or more overlapping *Chandra* fields, we associate it with the field that has a peak of SF at a look-back time consistent with its age (indicated in Column 4 of Table 1). This is necessary because we are measuring the SF history of each *Chandra* field.

Since our goal is to measure the formation rate of HMXBs as a function of the age of their parent stellar population, we first need to constrain the ages of the HMXBs and associate them with individual SF episodes responsible for the birth of their progenitors. Ages are derived from optical counterpart positions on the $(V, V-I)$ CMD with respect to the PARSEC isochrones (v1.2S; Bressan et al. 2012) generated by CMD 2.8⁵ for

⁴ Out of the 120 high-confidence sources reported in [HS16], only 65 fall within the 14 *Chandra* fields used in this work. Also, only 41 out of the 127 HMXB candidates in our survey have a match in the catalog of [HS16], i.e. 86 candidate HMXBs from this work are not listed in [HS16]. These sources have a limiting L_X of $\sim 1.7 \times 10^{32} \text{ erg/s}$. Five additional sources from [HS16] are not included in our final list because they have only *RXTE* or *INTEGRAL* positions with $\gtrsim 100''$ uncertainties.

⁵ <http://stev.oapd.inaf.it/cmd>

$Z = 0.004$ (Figure 2). We note that due to their circumstellar disks the Be stars are intrinsically redder than B-type stars of the same spectral type. By comparing the $(V-I)$ colors of B and Be stars from the census of Bonanos et al. (2010), we have found that early [B0–B2], and mid [B2–B4] spectral-type Be stars (i.e. within the typical range of companions of known SMC HMXBs; e.g. McBride et al. 2008, Antoniou et al. 2009b, Maravelias et al. 2014) have reddening-corrected $(V-I)_o$ colors ~ 0.3 and $\sim 0.2 \text{ mag}$ redder, respectively, than B stars of the same spectral type⁶. This systematic displacement (also obvious in Figure 2) implies that a Be system appears redder than a B star due to its equatorial disk.

Furthermore, each optical counterpart is associated with a SF episode taking into account the fact that stars can be associated with a SF event that overlaps with the age-range of isochrones consistent with its location on the CMD. For example, the SF history of *Chandra* field DF11 shows two prominent peaks at 7 Myr and 42 Myr. Out of the 17 HMXBs of DF11 (14 with unique optical counterparts and 3 with two optical matches; Column 3 of Table 1) only one X-ray source has an optical counterpart with a location on the OGLE-III $(V, V-I)$ CMD consistent with the peak at 7 Myr, while the remaining 16 have ages consistent the peak at 42 Myr (Figure 2). The HMXB and SF age associations, together with the SFR, duration and total stellar mass of the relevant SF episode, are presented in Table 1. The stellar mass formed during the SF episode associated with each HMXB population is calculated by integrating the SF history during the period of the star-formation episode of interest in each relevant field. For simplicity we approximate each SF episode as a sequence of Gaussian events; generally 1-3 Gaussians are adequate to reproduce the evolution of the SFR during a SF event.

4. HMXB FORMATION EFFICIENCY

We derive three different metrics of the age-dependent formation efficiency of HMXBs, the number of HMXBs in different ages with respect to the: (a) number of OB stars, $N(\text{OBs})$, in their respective *Chandra* field; (b) SFR of their parent stellar population; and (c) stellar mass formed during the SF episode they are associated with. The OB stars are from the OGLE-III catalog (§3), while the SFRs as a function of age are from [HZ04] and are listed in Column 6 of Table 1. The age-dependence of these three different tracers of the HMXB formation rate is shown in Figure 3. We have grouped together *Chandra* fields that have similar ages (as indicated by the

⁶ For spectral types later than B4, the very small size of the Be star sample does not allow us to derive any conclusions.

Table 1. HMXB Populations and Formation Efficiency

Age Bin [Myr]	Field ID	HMXBs	SF burst			HMXB Formation Efficiency			
			Age [Myr]	Span [Myr]	Rate [$10^{-3} M_{\odot}/\text{yr}$]	M_{\star} [$10^5 M_{\odot}$]	SFR [$10^{-1} M_{\odot}/\text{yr}$] $^{-1}$	OB stars [10^{-4}]	M_{\star} [$10^{-6} M_{\odot}$] $^{-1}$
(1)	(2)	(3)	(4)	(5)	(6)	(7)	(8)	(9)	(10)
6	DF11	1	7	4	115^{+46}_{-53}	$3.6^{+3.0}_{-1.7}$	$1.3^{+1.6}_{-1.3}$	4.3 ± 4.3	$8.5^{+10.6}_{-8.5}$
	NGC346	1	5	$\sim 1-2$	56^{+40}_{-55}	$0.7^{+0.5}_{-0.7}$			
11	DF01	1	11	6	37^{+11}_{-10}	$2.1^{+1.0}_{-0.6}$	5.5 ± 3.2	63 ± 33	$7.5^{+4.9}_{-4.4}$
	DF02	0	11	6	80 ± 14	$4.5^{+2.1}_{-1.2}$			
	DF03	5	11	6	73^{+10}_{-12}	$3.9^{+1.0}_{-0.8}$			
	DF04	4	11	6	57 ± 8	$3.2^{+1.1}_{-0.6}$			
34	DF05	5	34	43	30^{+6}_{-5}	15^{+4}_{-3}	24^{+10}_{-11}	34 ± 12	$5.4^{+2.7}_{-2.6}$
	DF06	11	34	36	37^{+9}_{-7}	16^{+6}_{-4}			
	DF07	11	34	34	42^{+10}_{-17}	18^{+7}_{-8}			
42	DF08	24	42	43	38 ± 5	18^{+3}_{-2}	49 ± 14	58 ± 15	12^{+5}_{-4}
	DF09	7	42	28	33 ± 6	$9.4^{+3.4}_{-2.1}$			
	DF11	16	42	22	53^{+9}_{-10}	16^{+7}_{-5}			
	DF01_A	18	42	30	37 ± 3	13 ± 2			
	DF02_A	27	42	41	25 ± 5	13^{+6}_{-5}			
	NGC346	7	42	30	37^{+5}_{-4}	11^{+3}_{-2}			
67	DF10	2	67	29	$2.7^{+6.9}_{-2.5}$	$7.2^{+3.4}_{-2.2}$	74^{+197}_{-74}	25 ± 18	$2.8^{+2.4}_{-2.1}$
266	DF02_A	1	266	436	$8.3^{+1.9}_{-1.7}$	68^{+9}_{-7}	12 ± 12	3.2 ± 3.2	0.1 ± 0.1

NOTE— Column (1): Average age (using values in Column 4) for the stellar populations in a given SF episode; Column (2): Field ID (Figure 1); Column (3): Number of HMXBs in each field associated with the respective SF episode; Columns (4) and (5): age and time-span (FWHM) of the dominant SF episode; Column (6): peak SFR of this episode (errors are based on the upper and lower SFR ranges reported by [HZ04]); Column (7): Total stellar mass (M_{\star}) produced in the SF episode (based on the integration of the SFR time-evolution); Columns (8), (9), (10): The HMXB formation efficiency based on the ratio of $N(\text{HMXBs})$ (Column 3) to the SFR (Column 6), the $N(\text{OBs})$, and the stellar mass (Column 7) produced during the SF burst they are associated with (see §3).

different group of fields shown in Table 1; e.g. DF05, DF06, and DF07, all showing a prominent peak in their SF histories at ~ 34 Myr). The error bars in the x-axis indicate the average age range of the stellar populations in each age bin.

The $N(\text{HMXBs})/N(\text{OBs})$ ratio shows a steep increase (by about an order of magnitude) from ~ 6 to 10 Myr, then a flattening up to ~ 60 Myr, followed by a drop (by about an order of magnitude again) for ages older than ~ 60 Myr.

On the other hand, the $N(\text{HMXBs})/\text{SFR}$ ratio increases rapidly up to ~ 40 –60 Myr, and then gradually decreases for older stellar populations. This result is consistent with previous lower age-resolution small-scale studies (involving shallow *Chandra* and *XMM-Newton* observations), which show an increased formation efficiency of HMXBs at ages between 30–60 Myr (of fields across the SMC Bar) compared to younger stellar populations (SMC Wing) (Shtykovskiy & Gilfanov 2005; Antoniou et al. 2009a).

The $N(\text{HMXBs})/M_\star$ ratio instead remains flat up to ~ 60 Myr, but it decreases for later ages as well. The data points averaged in the second age bin (at 11 Myr) correspond to fields that lie across the SMC Wing (Figure 1), one of the youngest identified SMC regions [HZ04]. These fields, although they have large SFRs (Table 1), they show SF episodes of small duration. This results in a small stellar mass formed, resulting in turn in a large $N(\text{HMXBs})/M_\star$ ratio. The same argument holds for the similar behavior of the $N(\text{HMXBs})/N(\text{OBs})$ ratio (which is effectively a proxy for stellar mass in massive stars).

An alternative formulation of the time taken for the formation of a class of astronomical objects (in this case, HMXBs) from the SF event that gives rise to its progenitor stellar systems is described by the Delay Time Distribution (DTD). The DTD is defined as the production rate of objects as a function of time after an hypothetical brief SF burst. Badenes et al. (2015) (hereafter [B15]) described a method to recover the DTD from an object catalog and a SF history map, and applied it to LMC planetary nebulae. Here, we apply the same method to the SMC HMXB catalog described in §3. The only difference with respect to the [B15] analysis is that the *Chandra* fields we used to derive the HMXB catalog do not cover a contiguous or uniform part of the SMC, and in many cases there is only partial overlap between a given *Chandra* field and a specific MCPS subregion. For this reason, we multiplied the SFR of each MCPS subregion in the SF history map of [HZ04] by a weight between 0 and 1, which represents the fraction of the

surface area of the subregion covered by *Chandra* (as was done in §3).

The resulting DTD is presented in Figure 4. We have used the temporal binning that offers the best compromise between DTD resolution and detection significance, given $N(\text{HMXBs})$ and the native resolution of the SF history map. We detect significant signal in the DTD of HMXB progenitors for stellar ages 21–53 Myr, and 53–84 Myr. Stellar populations in this age range generate $\sim 2 \times 10^{-5}$ HMXBs per unit stellar mass. This formation efficiency, ΨT_{HMXB} , is the product of the specific HMXB formation rate, Ψ [HMXBs $\text{yr}^{-1} M_\odot^{-1}$], and mean HMXB lifetime, T_{HMXB} [yr] —see Eqs. (1)–(3) and §2 in [B15]. For stellar populations younger than 21 Myr, we obtain a shallow 2σ upper limit to the HMXB formation efficiency of $\sim 2.3 \times 10^{-5} M_\odot^{-1}$. For stellar populations older than 84 Myr, we obtain a much lower upper limit of $2.5 \times 10^{-7} M_\odot^{-1}$. This indicates that there must be a maximum delay time for HMXB formation of less than 84 Myr, but longer than 53 Myr, given the significant detection in this bin.

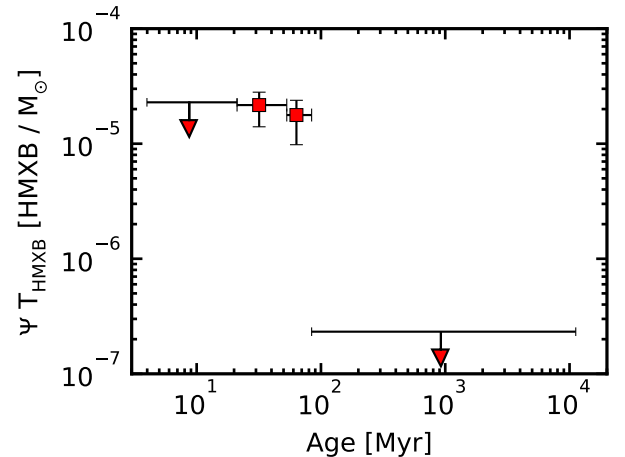


Figure 4. HMXBs Delay Time Distribution (following [B15]).

5. DISCUSSION

In section §4 we presented an analysis of the formation efficiency of HMXBs in the SMC based on a set of deep *Chandra* observations of this galaxy. We calculate this based on three different indicators, ($N(\text{HMXBs})/\text{SFR}$, $N(\text{HMXBs})/N(\text{OBs})$, and $N(\text{HMXBs})/M_\star$, all as a function of the age of the major associated SF burst), as well at the delay function formulation. We find that there is an increase in the formation rate for ages $\gtrsim 10$ –20 Myr and up to 40–60 Myr followed by a decline at older ages. The three HMXB formation efficiency indicators presented in Figure 3 serve different purposes.

$N(\text{HMXBs})/N(\text{OBs})$ is observationally driven, and takes into account the present-day numbers of OB stars. However, it does not take into account the donor star rejuvenation due to the first mass transfer from the initially more massive star that subsequently explodes as a SN and leaves behind a neutron star (or a black hole). Because of this rejuvenation, the system will live longer than single stars of similar mass formed during the same SF episode. This discrepancy is smaller for SF episodes of similar or longer duration compared to the lifetime of HMXB systems. Nonetheless, the $N(\text{HMXBs})/N(\text{OBs})$ ratio is an indicator that can be calculated directly for any nearby galaxy with resolved stellar populations, without the need to derive their SF history. Therefore, it serves as a useful proxy of the relative formation rate of HMXBs that can be applied to large samples of galaxies.

$N(\text{HMXBs})/\text{SFR}$ is based on the SF episode of the parent stellar population. It takes into account the SF event that created the binaries we observe today, but not the duration of the SF burst. In this work, we derived a peak formation efficiency $N(\text{HMXB})/\text{SFR}$ of $(49 \pm 14) [10^{-5} \text{ M}_{\odot}/\text{yr}]^{-1}$, in good agreement with previous estimates of the average formation efficiency in the broad $\sim 20\text{--}60$ Myr age range. We also find a factor of 8 rise in the formation efficiency with respect to younger populations (~ 10 Myr) and a factor of 4 decline in older epochs (~ 260 Myr). The different behavior of the $N(\text{HMXBs})/\text{SFR}$ with respect to the $N(\text{HMXBs})/N(\text{OBs})$ indicator could be the result of the age dependence of $N(\text{OBs})$: as the stellar populations age, a smaller number of OB stars is expected to be present. From a simple stellar lifetime argument folded through the IMF, the number of OB stars will be reduced with time, while the rejuvenation of the donor star would result in a longer lifetime of the binary systems. While $N(\text{HMXBs})/\text{SFR}$ is considered a more accurate representation of the formation efficiency of young accreting binaries than $N(\text{HMXBs})/N(\text{OBs})$, it is similarly problematic for providing observational constraints in sophisticated population synthesis models (e.g. Andrews et al. 2018).

More suitable is the ratio of $N(\text{HMXBs})$ to the total stellar mass produced in the relevant SF burst, since this takes into account the SF burst duration (the integral of the SFR as a function of time). This is the fundamental relation that we were aiming to derive from this *Chandra* XVP program, and the one that best resembles the delay function of the HMXBs. In fact, our $N(\text{HMXBs})/M_{\star}$ indicator (black points in Figure 3) is consistent (within the errors) with the DTD (shown in Figure 4). Moreover, our results are in good qualitative agreement with the simulated stellar-mass normalized

total X-ray luminosity output of a galaxy as a function of age of Fragos et al. (2013), who find an increase at ages $\gtrsim 20$ Myr and a decrease at ages $\lesssim 80$ Myr. This effect becomes more prominent in metallicities like those of the SMC ($1/5Z_{\odot}$).

The *Chandra* fields along the SMC Wing (DF01–DF04 in Figure 1) produce only a small number of HMXBs based on the surveys conducted so far (McGowan et al. 2008; Antoniou et al., in prep.). We attribute this deficiency on the strong but very recent (<10 Myr) star formation of the fields in this area (Antoniou et al. 2010) compared to the SMC Bar regions (typically $\sim 25\text{--}60$ Myr). Although this deficit might indicate an elusive, young, population of HMXBs, such as highly absorbed HMXBs (e.g. Walter et al. 2015), based on XRB evolution models we would expect a small number of XRBs at such young ages as only the most massive systems would have produced compact objects (Belczynski et al. 2008). Because of the large mass of the progenitors of these systems and the low metallicity of the SMC, we would expect these systems to be predominantly black-hole XRBs (Antoniou et al. 2010).

The time-resolved HMXB formation efficiency with respect to the stellar mass presented in Figure 3 is in good agreement with the general trend estimated by Shtykovskiy & Gilfanov (2007), who find a peak at similar ages (~ 40 Myr; albeit with coarser time resolution). We attribute differences in the absolute value of the formation efficiency in the two works to the fact that Shtykovskiy & Gilfanov (2007) consider only massive stars ($M > 8M_{\odot}$) in their calculation of stellar mass that was used to normalize the number of HMXBs.

Our results are also in agreement with studies of the formation efficiency of massive Oe/Be stars in the Magellanic Clouds (e.g. Martayan et al. 2006, Martayan et al. 2007, Bonanos et al. 2009, Bonanos et al. 2010), and the Milky Way (McSwain & Gies 2005). These show a peak at ages of $\sim 20\text{--}50$ Myr, matching the age of maximum production of HMXBs at least at the metallicity of the SMC. This similarity could indicate that: (a) the Be stars, the donor stars of Be-XRBs (the predominant HMXB population in the SMC), are the result of binary evolution (e.g. Porter & Rivinius 2003, and references therein), and/or (b) the larger mass-loss rates of Be stars through their equatorial winds (in comparison to the much weaker spherical stellar winds) lead to an enhanced population of active XRBs (c.f. Antoniou et al. 2010). However, only detailed population synthesis models accounting for the complex orbital evolution and mass-transfer in eccentric binaries (e.g. Dray 2006) can distinguish between these possibilities.

Finally, a first assessment of the overall XRB formation rate in the LMC, which has two SF episodes at similar ages as the SMC (12.6 Myr and 42 Myr) but with different intensities, indicates that the formation efficiency of its overall XRB population is ~ 17 times lower than in the SMC (Antoniou & Zezas 2016). This could be the result of a metallicity effect (e.g. Be stars form more efficiently at lower metallicities as shown by Martayan et al. 2007 and Iqbal & Keller 2013). Furthermore, Dray (2006) finds that at the $\sim 1/5Z_{\odot}$ metallicity of the SMC, population synthesis models predict 3 times larger populations of HMXBs than in the Milky Way. However, only a more systematic study of the formation efficiency of XRBs in the higher metallicity LMC galaxy will show how it truly depends on the metallicity.

6. CONCLUSIONS

We have investigated the formation efficiency of HMXBs in the low SMC metallicity *for the first time* as a function of the age of their parent stellar population. We have used the different formation efficiency indicators $N(\text{HMXBs})/\text{SFR}$, $N(\text{HMXBs})/N(\text{OBs})$, and $N(\text{HMXBs})/M_{\star}$, all as a function of the age of the major associated SF burst. In all cases, we find an increase in the formation efficiency up to an age of $\sim 40\text{--}60$ Myr, and a gradual decrease thereafter. The peak formation efficiency $N(\text{HMXB})/\text{SFR}$ is estimated as $(49 \pm 14) [10^{-5} \text{ M}_{\odot}/\text{yr}]^{-1}$, in good agreement with previous estimates of the average formation efficiency in the broad $\sim 20\text{--}60$ Myr age range. This peak in the formation efficiency of the SMC HMXBs ($8\times$ and $4\times$ higher than at

earlier (~ 10 Myr), and later epochs (~ 260 Myr), respectively) is in excellent agreement with previous studies that have examined it on Be stars in both the Magellanic Clouds and the Milky Way.

ACKNOWLEDGEMENTS

We thank K. D. Kuntz for useful comments that have improved the quality of the paper. VA acknowledges financial support from NASA/Chandra grants GO3-14051X, AR4-15003X, NNX15AR30G, NASA/ADAP grant NNX10AH47G, and the Texas Tech President's Office. AZ acknowledges financial support from NASA/ADAP grant NNX12AN05G and funding from the European Research Council under the European Union's Seventh Framework Programme (FP/2007-2013)/ERC Grant Agreement n. 617001. This project has also received funding from the European Union's Horizon 2020 research and innovation programme under the Marie Skłodowska-Curie RISE action, grant agreement No 691164 (ASTROSTAT). JJD, TJG, and PPP were funded by NASA contract NAS8-03060 to the *Chandra X-ray Center*. PFW acknowledges financial support from the NSF through grant AST-1714281. The OGLE project has received funding from the National Science Centre, Poland, grant MAESTRO 2014/14/A/ST9/00121 to AU. We thank the CXC Director, Belinda Wilkes, for advice and support, and for funding the publication of this work. This research has made use of NASA's Astrophysics Data System and the Tool for OPERations on Catalogues And Tables (TOPCAT) software package (Taylor 2005).

REFERENCES

- Andrews, J. J., Zezas, A., & Fragos, T. 2018, ApJS, 237, 1
- Antoniou, V., Hatzidimitriou, D., Zezas, A., & Reig, P. 2009b, ApJ, 707, 1080
- Antoniou, V., & Zezas, A. 2016, MNRAS, 459, 528
- Antoniou, V., Zezas, A., Hatzidimitriou, D., & Kalogera, V. 2010, ApJL, 716, L140
- Antoniou, V., Zezas, A., Hatzidimitriou, D., & McDowell, J. C. 2009a, ApJ, 697, 1695
- Badenes, C., Maoz, D., & Ciardullo, R. 2015, ApJL, 804, L25
- Belczynski, K., Kalogera, V., Rasio, F. A., et al. 2008, ApJS, 174, 223-260
- Bonanos, A. Z., Massa, D. L., Sewilo, M., et al. 2009, AJ, 138, 1003
- Bonanos, A. Z., Lennon, D. J., Köhlinger, F., et al. 2010, AJ, 140, 416
- Bressan, A., Marigo, P., Girardi, L., et al. 2012, MNRAS, 427, 127
- Broos P. S., Townsley L. K., Feigelson E. D., Getman K. V., Bauer F. E., Garmire G. P., 2010, ApJ, 714, 1582
- Broos P., Townsley L., Getman K., Bauer F., 2012, ascl.soft, 1203.001
- Cardelli, J. A., Clayton, G. C., & Mathis, J. S. 1989, ApJ, 345, 245
- Coe, M. J., & Kirk, J. 2015, MNRAS, 452, 969
- Corbet, R. H. D., Coe, M. J., McGowan, K. E., et al. 2009, The Magellanic System: Stars, Gas, and Galaxies, 256, 361
- de Grijs, R., & Bono, G. 2015, AJ, 149, 179
- Dray, L. M. 2006, MNRAS, 370, 2079
- Frags, T., Lehmer, B., Tremmel, M., et al. 2013, ApJ, 764, 41

- Gordon, K. D., Clayton, G. C., Misselt, K. A., Landolt, A. U., & Wolff, M. J. 2003, *ApJ*, 594, 279
- Grimm, H.-J., Gilfanov, M., & Sunyaev, R. 2003, *MNRAS*, 339, 793
- Haberl, F., Filipović, M. D., Pietsch, W., & Kahabka, P. 2000, *A&AS*, 142, 41
- Haberl, F., Sturm, R., Ballet, J., et al. 2012, *A&A*, 545, A128
- Haberl, F., & Sturm, R. 2016, *A&A*, 586, A81
- Harris J., Zaritsky D., 2004, *AJ*, 127, 1531
- Harrison, F. A., Craig, W. W., Christensen, F. E., et al. 2013, *ApJ*, 770, 103
- Hong, J., van den Berg, M., Schlegel, E. M., et al. 2005, *ApJ*, 635, 907
- Hong, J., Antoniou, V., Zezas, A., et al. 2016, *ApJ*, 826, 4
- Hong, J., Antoniou, V., Zezas, A., et al. 2017, *ApJ*, 847, 26
- Iqbal, S., & Keller, S. C. 2013, *MNRAS*, 435, 3103
- Laycock, S., Corbet, R. H. D., Coe, M. J., et al. 2005, *ApJS*, 161, 96
- Laycock S., Zezas A., Hong J., Drake J. J., Antoniou V., 2010, *ApJ*, 716, 1217
- Lehmer, B. D., Alexander, D. M., Bauer, F. E., et al. 2010, *ApJ*, 724, 559
- Lehmer, B. D., Basu-Zych, A. R., Mineo, S., et al. 2016, *ApJ*, 825, 7
- Linden, T., Kalogera, V., Sepinsky, J. F., et al. 2010, *ApJ*, 725, 1984
- Luck, R. E., Moffett, T. J., Barnes, T. G., III, & Gieren, W. P. 1998, *AJ*, 115, 605
- Maravelias, G., Zezas, A., Antoniou, V., & Hatzidimitriou, D. 2014, *MNRAS*, 438, 2005
- Martayan, C., Frémat, Y., Hubert, A.-M., et al. 2006, *A&A*, 452, 273
- Martayan, C., Floquet, M., Hubert, A. M., et al. 2007, *A&A*, 472, 577
- Martayan, C., Frémat, Y., Hubert, A.-M., et al. 2007, *A&A*, 462, 683
- McBride, V. A., Coe, M. J., Negueruela, I., Schurch, M. P. E., & McGowan, K. E. 2008, *MNRAS*, 388, 1198
- McGowan, K. E., Coe, M. J., Schurch, M. P. E., et al. 2008, *MNRAS*, 383, 330
- McSwain, M. V., & Gies, D. R. 2005, *ApJS*, 161, 118
- Mineo, S., Gilfanov, M., & Sunyaev, R. 2012, *MNRAS*, 419, 2095
- Nazé Y., Hartwell J. M., Stevens I. R., Corcoran M. F., Chu Y.-H., Koenigsberger G., Moffat A. F. J., Niemela V. S., 2002, *ApJ*, 580, 225
- Porter, J. M., & Rivinius, T. 2003, *PASP*, 115, 1153
- Sasaki, M., Haberl, F., & Pietsch, W. 2000, *A&AS*, 147, 75
- Seward, F. D., & Mitchell, M. 1981, *ApJ*, 243, 736
- Shtykovskiy, P., & Gilfanov, M. 2005, *A&A*, 431, 597
- Shtykovskiy, P. E., & Gilfanov, M. R. 2007, *Astronomy Letters*, 33, 437
- Sturm, R., Haberl, F., Pietsch, W., et al. 2013, *A&A*, 558, A3
- Taylor, M. B. 2005, *Astronomical Data Analysis Software and Systems XIV*, 347, 29
- Udalski, A., Soszynski, I., Szymanski, M., et al. 1999, *AcA*, 49, 437
- Udalski, A., Soszyński, I., Szymański, M. K., et al. 2008, *AcA*, 58, 329
- Walter, R., Lutovinov, A. A., Bozzo, E., & Tsygankov, S. S. 2015, *A&A Rv*, 23, 2
- Williams, B. F., Binder, B. A., Dalcanton, J. J., Eracleous, M., & Dolphin, A. 2013, *ApJ*, 772, 12
- Yokogawa, J., Imanishi, K., Tsujimoto, M., Koyama, K., & Nishiuchi, M. 2003, *PASJ*, 55, 161